

## The improvement of cross-calibration of IIM data and band selection for FeO inversion

WANG Chao<sup>1,2</sup>, WU YunZhao<sup>3</sup>, SHI RunHe<sup>1,2\*</sup> & GAO Wei<sup>1,2</sup>

<sup>1</sup>Key Laboratory of Geographical Information Science, Ministry of Education, East China Normal University, Shanghai 200062, China;

<sup>2</sup>Branch of Data Application System, Center of Space Exploration, Ministry of Education, East China Normal University, Shanghai 200062, China;

<sup>3</sup>School of Geographic and Oceanographic Sciences, Nanjing University, Nanjing 210093, China

Received December 30, 2012; accepted March 7, 2013; published online July 10, 2013

Chang'E-1 (CE-1) Interference Imaging Spectrometer (IIM) dataset suffers from the weak response in the near infrared (NIR) bands, which are the important wavelength for retrieving the minerals and elements of the Moon. In this paper, the cross-calibration was implemented to the IIM hyperspectral data for improving the weak response in NIR bands. The results show that the cross-calibrated IIM spectra were consistent to the Earth-based telescopic spectra, which suggests that the cross-calibration yields acceptable results. For further validating the influence of the cross-calibration on the FeO inversion and searching the optimal bands to retrieve lunar FeO contents, four band selection schemes were designed to retrieve FeO using the original and cross-calibrated IIM spectra. By comparing the distribution patterns and histograms of the IIM derived FeO contents with the Clementine derived FeO, the IIM 891 nm band after cross-calibration showed a higher accuracy in the FeO inversion, hence most useful for lunar FeO inversion.

**IIM, cross-calibration, band selection, FeO, Moon**

**PACS number(s):** 95.55.Pe, 95.75.Mn, 95.85.-e, 96.12.Ma

**Citation:** Wang C, Wu Y Z, Shi R H, et al. The improvement of cross-calibration of IIM data and band selection for FeO inversion. *Sci China-Phys Mech Astron*, 2013, 56: 2216–2225, doi: 10.1007/s11433-013-5172-8

The Interference Imaging Spectrometer (IIM) is one of the eight payloads onboard Chang'E-1 (CE-1), the Chinese first satellite to orbit the Moon. The spectrometer is a Sagnac-based spatially modulated Fourier transform imaging device that uses an interference pattern to derive spectra, and was designed to obtain spectral information and analyze the composition of lunar surface. IIM is the first planetary application of interference imaging technology [1,2].

Preprocessing of remote sensing data is crucial before the application in scientific research. Many researchers studied the preprocessing of IIM data since the data had been released. The reflectance spectrum of Apollo 16 soil 62231 measured in the laboratory and the corresponding area of

undisturbed soil of Apollo 16 sites have been often used for the calibration of lunar remote sensing data [3–5]. This method was also used in IIM data reduction [6]. Bad pixels, bad samples and vertical stripes in IIM data were detected and corrected [7]. The inhomogeneity of IIM sensor response in the line direction was found and corrected by the method termed reflectance normalization [6,8]. Based on the past experience and the understanding of IIM, a new photometric correction and in-flight calibration method have been proposed recently [9]. The new method calculated the radiance factor (RADF), a critical variable in photometric model, by utilizing the solar spectrum and normalizing the Sun-Moon distance. A second innovation of the new model is that it decoupled the combined effects of the solar photometry and the detector responsivity along the cross-

\*Corresponding author (email: shirunhe@gmail.com)

track. The global lunar reflectance in standard geometric condition ( $i=30^\circ$ ,  $e=0^\circ$ ,  $\alpha=30^\circ$ ) was subsequently generated from the newly calibrated IIM data. The IIM near infrared (NIR) bands have weak response, which has confined the application in scientific research. For instance, FeO inversion and identification of mafic minerals was not accurate because the absorption center of lunar mafic minerals is near 1000 nm. Therefore, further calibration for the newly processed IIM data is needed to improve its applicability. Cross-calibration for IIM NIR bands has been developed [10]. However, the applicability is limited because the telescopic spectra are inadequate. Only six sites were selected for cross-calibration. In this paper, the cross-calibration was performed on newly processed IIM reflectance data [9] and the procedure was improved by importing large amounts of telescopic spectra [11] into the computation of cross-calibration factors and controlling the quality of the telescopic spectra strictly for insuring the precision of the cross-calibration.

Iron is one of the principal elements that dominate the spectral features of the Moon and has a great significance by contributing to the understanding of the diagenetic process and the thermal history of the Moon [12,13]. It is also the supplementary information to retrieve some other elements, such as Gd and Sm [14]. Only a small part of the Moon surface can be investigated by using the lunar samples returned from the Luna and Apollo missions, therefore, remote sensing is still the primary technology in terms of retrieving the FeO abundance and distribution in large scale in both regional and global scale. Clementine multispectral data have been used to retrieve lunar FeO contents. The bands of Clementine multispectral data used for FeO prediction are 750 nm band in visible (VIS) and 950 nm band in NIR. Many researchers have attempted to use IIM data to retrieve the lunar FeO abundance. With regard to the IIM VIS and NIR bands used for FeO retrieval, there are two types of band selection schemes. One scheme used by Ling et al. [15], is that 757 nm for VIS and 891 nm for NIR band. The other scheme is 757 nm for VIS and 918 nm for NIR used by Wu et al. [10] and Yan et al. [16]. Cross-calibration has not been implemented to IIM in the former scheme, and in the latter scheme, cross-calibration was performed to IIM data to elevate the NIR response. There has not been any research focusing on which bands are considered optimal for FeO inversion. In order to explore the optimal bands for the inversion of FeO and validate whether cross-calibration of the IIM NIR bands is useful to improve the retrieval precision, four IIM band selection schemes to retrieve FeO content were tested. The work in this paper is useful for improving the applicability and precision of IIM.

## 1 Data source

CE-1 IIM began to collect the lunar spectral information on

Nov. 27th, 2007 and was guided to crash into the Moon on Mar. 1st, 2009. The collected hyperspectral data approximately cover the 78% area of the Moon. The IIM data were received, processed and distributed by the Ground Segment for Data Science and Application (GSDSA). Some key characteristics of IIM are shown in Table 1. Detailed description can be found elsewhere [11,17]. The IIM level 2A data were used here.

## 2 Methodology

### 2.1 Data processing

The IIM 2A data need to be processed before application. In this paper, the IIM data processing contains the following steps: 1) Band investigation; some bands of IIM data suffer from large noise. The bands at 480 nm, 488 nm, 496 nm, 504 nm, 513 nm and 946 nm were excluded. 2) Reflectance conversion; the radiance was converted into reflectance as performed previously [3]. 3) Bad pixel correction; the IIM data contain some bad pixels which increased the standard deviation of images. Wu et al. [9] corrections to the pixels were used. 4) In-flight flat-field correction and photometric correction; the inhomogeneity of sensor response has been corrected and a global lunar reflectance map whose boundaries between adjacent orbits are invisible was generated after photometric correction. Further details regarding flat-field correction and photometric correction can be found elsewhere [9].

### 2.2 Cross-calibration

The referenced spectra were obtained by Earth-based telescopes, which is located at an elevation of almost 4200 m at Mauna Kea Observatory (MKO) in Hawaii, USA. It has a high quality in NIR bands because the observation provides two essential conditions for this Earth-based type data: firstly, sufficiently low atmospheric absorption to allow an adequate signal continuous spectral measurement to 2.5  $\mu\text{m}$ , and secondly, good to excellent sighting capability [4]. The telescopic spectrum have a continuous wavelength coverage

**Table 1** Performance Characteristics of IIM

Index	Value
Spectral range (nm)	480–960
Spectral resolution ( $\text{cm}^{-1}$ )	330
Channels	32 bands
Swath width (km)	25.6
Spatial resolution (m)	200
Data coverage area	75°N–75°S
S/N	$\geq 100$
Digital Level (bit)	12
MTF	$\geq 0.2$
Orbit altitude (km)	200

from 0.65 to 2.5  $\mu\text{m}$  for small area on the lunar surface and it was provided by the Keck/NASA Reflectance Experiment Laboratory (RELAB) at Brown University, USA and archived by the PDS Geosciences Node (<http://geo.pds.nasa.gov/missions/lunarspec/index.htm>). By comparing IIM reflectance data with telescopic data, the IIM spectra show a lower response in NIR bands than telescopic spectra, particularly for 891 nm and 918 nm, but consistent in short wave bands. As mentioned above, NIR bands are critical for the inversion of FeO. Thus the weak response in NIR bands should be corrected before applying IIM data to chemical compositions retrieval.

As in previous studies [10], the telescopic spectra used for cross-calibration is insufficient to represent the global lunar surface and various landforms. In this research, all the telescopic spectra in PDS node [4] were checked, and the high-quality data were chosen to be involved in the computation of the cross-calibration factors. At the same time, the quality of IIM data should also be guaranteed and the data should cover the same areas where telescope measured. After careful selection, twenty-two telescopic spectra were chosen and used for the computation. The information of the telescopic spectra chosen in this research is shown in Figure 1 and Table 2.

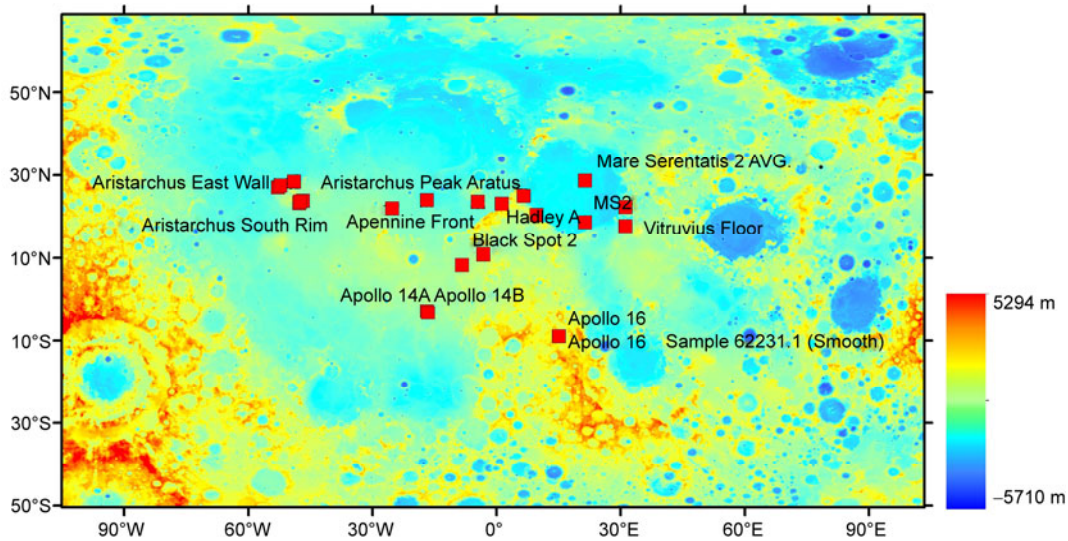


**Figure 1** Location of the 22 telescopic spectra on the map of the lunar DEM derived from CE-1 CCD.

**Table 2** Summary information of sites used in IIM cross-calibration

Sites name	Telescopic spectral ID	IIM Revolution	IIM location (sample, line)	Lat./Long.	Feature type
Sulpicius Gallus 2	HA1055	2230	72, 6701	20.4N, 9.7E	Mantling Material
Apennine Front	HA0819	2856	53, 7620	23.1N, 1.3E	Mountain
Sinus Aestuum 3	HA0857	2550	35, 9877	10.8N, 3.2W	Mare
Black Spot 2	HA1094	2864	84, 9923	8.3N, 8.3W	Mantling Material
Aristarchus Plateau 1	HA0979	2902	6, 7030	27.1N, 52.8W	Mantling Material
Vitruvius Floor	HA1088	2521	69, 8546	17.7N, 31.2E	Mare
MS2	HB0916	2220	72, 6929	18.7N, 21.4E	Mare
Apollo 16	H90366	2225	71, 11159	9.0S, 15.1E	Highlands
Aristarchus Plateau 2	HA0130	2902	47, 6948	28.4N, 48.9W	Mantling Material
Aristarchus Plateau 3	HA1032	2899	40, 6984	27.5N, 52.3W	Mantling Material
Hadley A	HA0811	2852	108, 7344	25.0N, 6.6E	Crater
Aristarchus South Rim	HA1040	2898	60, 7693	23.3N, 47.7W	Crater Feature (WALL)
Mare Serentatis 2 AVG.	HC0033	2220	86, 6915	28.7N, 21.4E	Mare
Litrow NR	HA1082	2521	67, 7840	22.3N, 31.2E	Mountain
Apollo 16 Sample 62231 (Smooth)	HC0028	2225	125, 11161	9S, 15.1E	Highlands
Apollo 14A	HC1192	2252	70, 10191	2.8S, 16.8W	Highlands
Apollo 14B	HC1194	2252	101, 10250	3.2S, 16.6W	Highlands
Copernicus Mare 5	HC0758	2569	39, 8357	22N, 25.2W	Mare
Copernicus Ray 6	HD0352	2562	61, 7800	24N, 16.8W	Crater Feature(Ray)
Aratus	HA0809	2853	3, 7661	23.6N, 4.5W	Crater(Highland)
Aristarchus East Wall	HA1038	2897	12, 7511	23.8N, 46.8W	Crater Feature (WALL)
Aristarchus Peak	HA0971	2898	90, 7598	23.7N, 47.5W	Central Peaks

Figure 1 shows the location of the 22 telescopic spectra used in the IIM cross-calibration procedure. As can be seen in Figure 1, the spectra are widely distributed on the near-side of the Moon, and covers various landforms, such as highland (Apollo 16, Apollo 14A), mare (Vitruvius Floor, MS2, Sinus Aestuum 3) and craters (Aratus, Aristarchus East Wall). The data used in ref. [10] were all included in this work. Table 2 contains the detailed information of the telescopic spectra, including telescopic spectral ID, the location of the telescopic spectra in IIM images, the feature type of each spectrum.

The cross-calibration procedure in this paper includes the following steps:

1) Transforming absolute reflectance into scaled reflectance. The telescopic spectra provided by PDS Geosciences node are scaled reflectance. In order to compare IIM spectra with telescopic data, the IIM absolute reflectance was also transformed into scaled reflectance, because both IIM and telescopic data have the 776 nm band. In this step, all bands of IIM data were scaled to unity 776 nm.

2) Spectral denoising. Cubic B spline fitting was applied to the telescopic spectra.

3) Spectral resampling. The telescopic spectra were resampled by using a Gaussian model according to the wavelength and full-width-at-half-max (FWHM), because of their different central wavelength to IIM.

4) Deriving the gain and offset. The gain and offset were found with least squares method. The formula used for computing the gain and offset is given as:

$$R_{\text{Tele}}^{\lambda} = G^{\lambda} \times R_{\text{IIM}}^{\lambda} + O^{\lambda}, \quad (1)$$

where the  $R_{\text{Tele}}^{\lambda}$  is the telescopic spectra scaled reflectance in  $\lambda$  band,  $R_{\text{IIM}}^{\lambda}$  is the IIM spectra scaled reflectance in  $\lambda$  band,  $G^{\lambda}$  and  $O^{\lambda}$  represent the gain and offset in  $\lambda$  band. Note the difference between this formula and the method given elsewhere [10].

### 2.3 Band selection for FeO inversion

Many models have been developed to measure lunar FeO contents. These models can be classified into two types. One approach is to build a statistical relationship between remote sensing data and compositional data to retrieve the FeO contents such as principal component analysis [18], partial least square regression [19], and support vector machine [20]. These methods are purely mathematical and show potential of FeO inversion with reflectance spectra. However, their accuracy is limited because of the insufficient sampling data when apply the statistical relationship to large regions. The other algorithm proposed by Lucey et al. [12,21,22] parameterizes the spectral properties sensitive to iron and soil maturity, and explicitly minimizes artifacts at the global scale. This model was widely used because of its clearly physical mechanism [11,15,16,23]. In this paper, this

method was adopted to retrieve FeO content. The key to the Fe parameter  $\theta_{\text{Fe}}$ , the location of the ‘hypermaturation’ end-member in the plot of NIR/VIS versus VIS reflectance can be determined by the suggestion of Lucey et al. [22], that is maximizing the correlation between remotely measured parameter  $\theta_{\text{Fe}}$  and the FeO contents of the sample soils and minimizing the residual effects of maturity. The  $\theta_{\text{Fe}}$  is calculated on the basis of the location of the end-member as:

$$\theta_{\text{Fe}} = -\arctan \left\{ \frac{R_{\text{NIR}}/R_{\text{VIS}} - A}{R_{\text{VIS}} - B} \right\}, \quad (2)$$

where  $A$  and  $B$  are the NIR/VIS ratio and VIS reflectance of the end-member, respectively.  $R_{\text{NIR}}$  and  $R_{\text{VIS}}$  are the reflectance in NIR band and VIS band. After computation of the  $\theta_{\text{Fe}}$ , a power function was found between  $\theta_{\text{Fe}}$  and FeO contents of sample soils [10]. Then the FeO contents can be derived by

$$\text{wt\%FeO} = C \times \theta_{\text{Fe}}^D, \quad (3)$$

where  $C$  and  $D$  can be obtained by regression of  $\theta_{\text{Fe}}$  and FeO contents of sample soils. The sample soils data were referenced elsewhere [10].

The determination of the VIS and NIR bands for FeO inversion is critical [24]. As shown above, previous research regarding FeO inversion using IIM data show only the selected VIS and NIR bands, while not showing the detailed band selection process. There are two types of band selection schemes. One scheme in Ling et al. [15] is 757 nm and 891 nm bands after absolute calibration without performing cross-calibration. The other scheme is 757 nm and 918 nm [11,16] which have performed cross-calibration to the original IIM reflectance. The VIS bands chosen are identical, but differences do exist in terms of the NIR bands they chose. In order to confirm the most suitable band for the FeO inversion and validate the influence of the cross-calibration, four band selection schemes were designed to retrieve FeO contents using IIM data (Table 3).

## 3 Results

### 3.1 Cross-calibration

Figure 2 shows the comparison among original IIM spectra (“uncorrect IIM”), telescopic spectra (“Telescope”) and

**Table 3** Band selection schemes for FeO retrieval using IIM data

		VIS (nm)	NIR (nm)
1	Original	757	891
2		757	918
3	Cross-calibrated	757	891
4		757	918

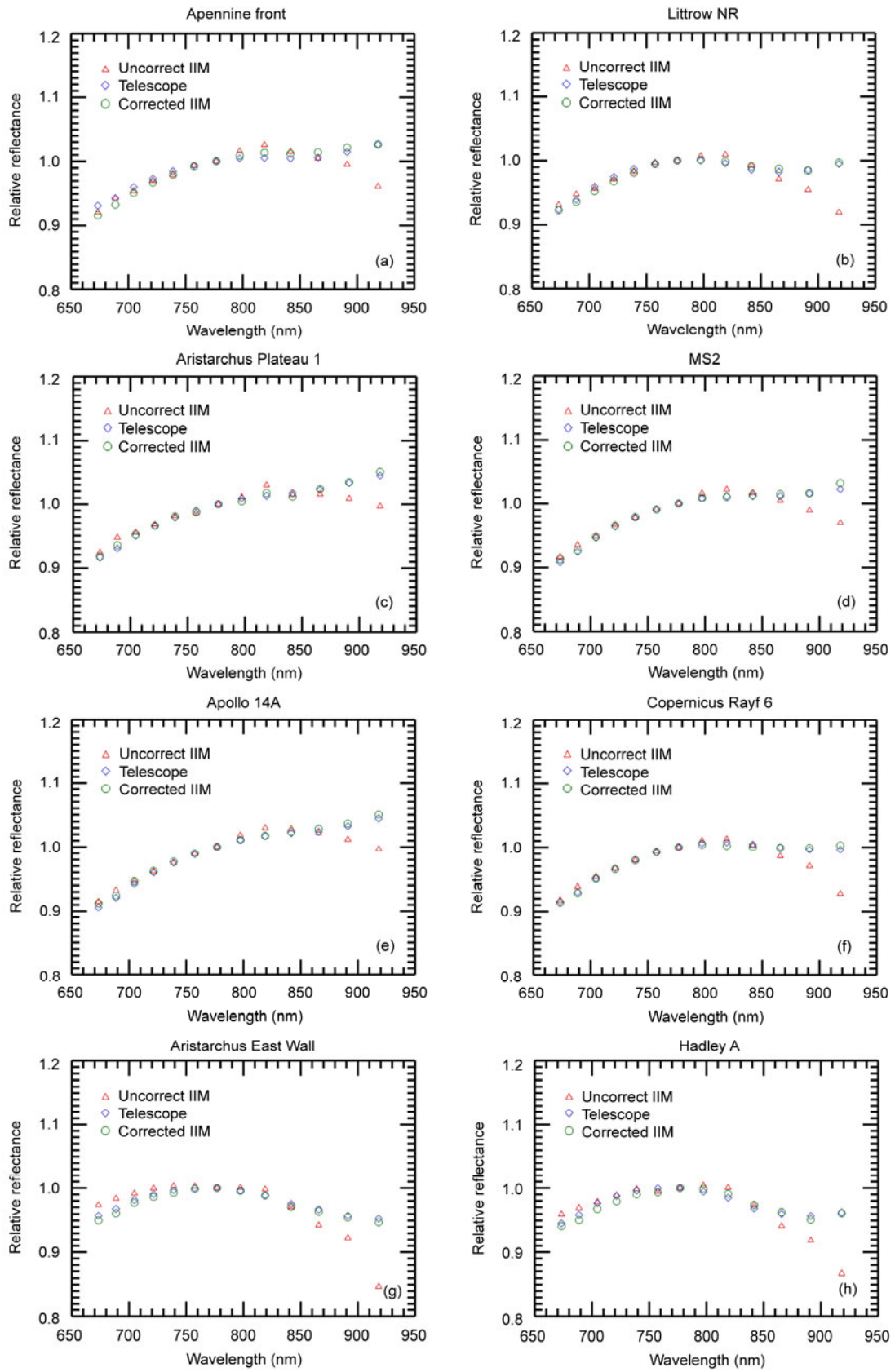


**Figure 2** (Color online) Comparison of telescopic spectra and IIM spectra in Apennine Front (a), Littrow NR (b), Aristarchus Plateau 1 (c), MS2 (d), Apollo 14A (e), Copernicus Ray 6 (f), Aristarchus East Wall (g) and Hadley A (h).

cross-calibrated IIM spectra (“corrected IIM”). Because of the limitations of the paper, only eight sites involved in cross-calibration procedure were demonstrated. The eight sites are Apennine Front, Aristarchus Plateau 1, MS2, Hadley A, Littrow NR, Apollo 14A, Copernicus Ray 6 and Aristarchus East Wall. They represent various feature types, such as Mountain, Mantling Material, Mare, Crater, Mountain, Highlands, Crater Feature (Ray) and Crater Feature (WALL). It can be seen that the original IIM reflectance is lower than telescopic spectra at long wave bands (e.g., 891 nm and 918 nm), but after cross-calibration, telescopic and cross-calibrated IIM spectra are consistent in the mutual spectral ranges. The reflectance at long wave bands is greatly improved, particularly at 891 nm and 918 nm. Simultaneously, the original spectral characteristics in short wave bands were reserved in cross-calibration. Table 4 shows the cross-calibration factors and statistical information before and after cross-calibration. The root mean square error (RMSE) in Table 4 is defined by

$$\text{RMSE} = \sqrt{(R_{\text{Tele}}^{\lambda} / IR_{\text{Tele}}^{776} - F_{\text{IIM}}^{\lambda} / IR_{\text{IIM}}^{776})^2 / N}, \quad (4)$$

where  $N$  is the number of telescopic measure sites. The RMSE (Table 4) in each band decreased significantly after cross-calibration, particularly at 891 nm and 918 nm, which are the bands of most concern in this research. They decreased by 62.8% and 74.1%, respectively. The correlation coefficients between corrected IIM reflectance data and telescopic spectra in each band are greater than 0.8, indicating a well correlation. Figures 3(a) and (b) show the composite images of 918 nm (R), 776 nm (G) and 618 nm (B) of the Aristarchus crater area and Figures 3(c) and (d) for the Vaisala crater area. A striking difference between Figures 3(a) and (b) or Figures 3(c) and (d) is that the blue (indicating soil immaturity) of fresh surface or ejecta become weakened, which suggests that the response of 918 nm band has improved.

### 3.2 IIM band selection for FeO inversion

The derivation of the location of the ‘hypermaturation’ end-member is very important for the inversion accuracy [22]. The end-member is located in the low VIS reflectance and high NIR/VIS ratio portion of the ratio-reflectance plot (Figure 4), which represents the convergence of maturity trends for lunar materials with differing iron contents [22]. There are many possible locations in the ratio-reflectance plot. Figure 4 shows the location of the ‘hypermaturation’ end-members of the four band selection schemes as accorded in Table 3. In order to avoid the negative retrieval value, 5000 pixels were plotted as the ‘background value’ [25]. The 5000 pixels were randomly extracted from IIM data.

After the careful selection of the ‘hypermaturation’ end-members, the four parameters in eqs. (2) and (3) were obtained. The parameters in eqs. (2) and (3) and correlation coefficients between the FeO contents measured from sample soils and the FeO contents retrieved from the IIM data are listed in Table 5.

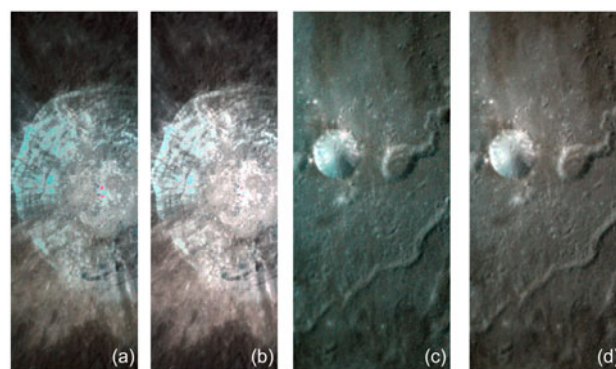


**Figure 3** Composite images of 918 nm (R), 776 nm (G) and 618 nm (B) of the IIM reflectance data for Aristarchus crater area ((a) and (b)) and Vaisala crater area ((c) and (d)). (a) and (c) are the original composite images and (b) and (d) are the composite images after cross-calibrating.

**Table 4** The cross-calibration factors of IIM and statistic information before and after cross-calibration

Band (nm)	Gain	Offset	RMSE (Before)	RMSE (After)	$R^a$
673	0.6514	0.3161	0.0132	0.0070	0.9091
688	0.7249	0.2483	0.0148	0.0065	0.9066
704	0.6903	0.2924	0.0090	0.0061	0.8835
721	0.6345	0.3518	0.0080	0.0050	0.8756
738	0.5492	0.4416	0.0067	0.0040	0.8452
757	0.6630	0.3337	0.0029	0.0023	0.8068
797	0.8821	0.1128	0.0073	0.0030	0.8678
818	0.9149	0.0753	0.0126	0.0050	0.8976
841	0.9191	0.0787	0.0079	0.0070	0.9333
865	0.8179	0.1926	0.0140	0.0081	0.9445
891	0.9161	0.1098	0.0288	0.0107	0.9416
918	0.6883	0.3643	0.0684	0.0177	0.8801

a)  $R$ : correlation coefficient between IIM reflectance data and telescopic spectra in each band.

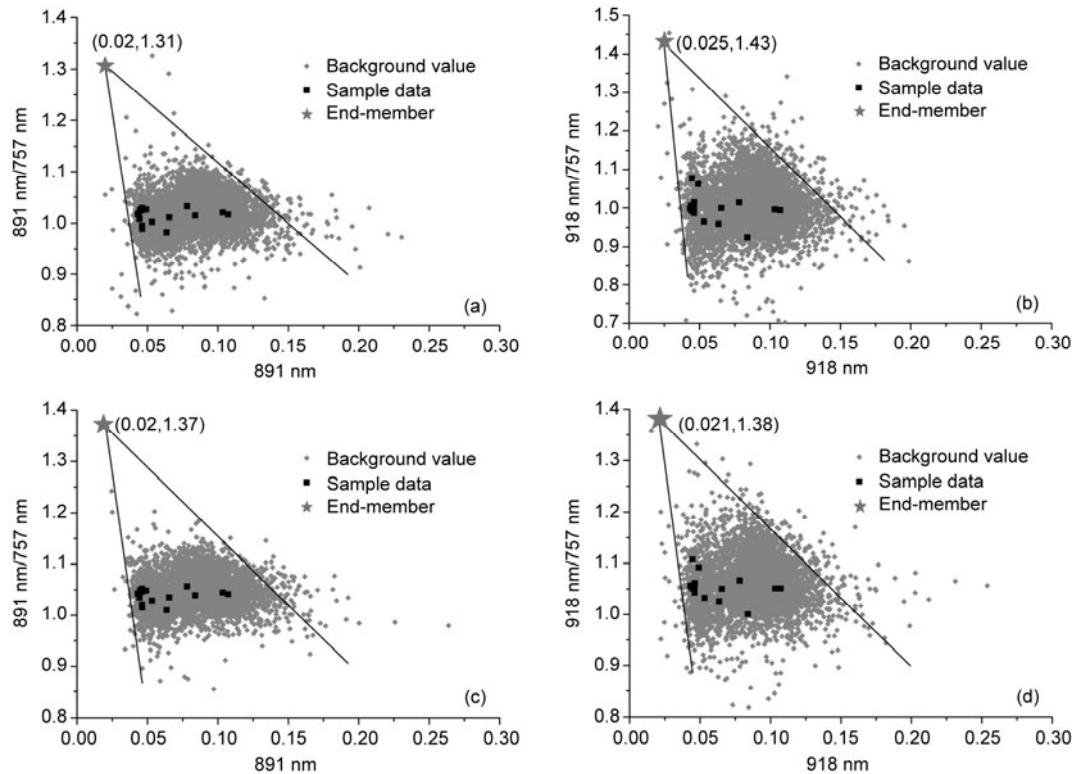


**Figure 4** Ratio-reflectance plots of background value, sample data and 'hypermaturation' end-member of the four schemes: (a) 757 nm and 891 nm without cross-calibration, (b) 757 nm and 918 nm without cross-calibration, (c) 757 nm and 891 nm with cross-calibration and (d) 757 nm and 918 nm with cross-calibration.

**Table 5** Parameters in eqs. (2) and (3) for the four schemes (Table 3) and correlation coefficients between FeO from samples and IIM

	Original		Cross-calibration	
	891 nm	918 nm	891 nm	918 nm
A	1.31	1.43	1.37	1.38
B	0.020	0.025	0.020	0.021
C	0.2400	0.0365	0.3069	0.2160
D	10.1955	14.5939	9.9503	10.8309
R	0.958	0.960	0.958	0.969

As shown in Table 5, the difference of the four correlation coefficients is insignificant. They are both near 0.96, while the value of the fourth coefficient is slightly larger than the others. However, the correlation coefficients only cannot affirm which scheme is the most suitable for the FeO inversion, because the sampling data used for statistic are insufficient. For validating the accuracy of the four schemes, the inversion model was applied in a large-scale area. The area where Oceanus Procellarum is located was chosen as the test area. Oceanus Procellarum is the largest mare of the Moon and represents the most widespread continuous deposit of mare basalts. It is situated in the west of the Moon nearside, but the sample-return sites concentrated on the east side of the Moon. At the current stage, the compositions information of Oceanus Procellarum can only be derived from remote sensing data.

The test area is shown in Figure 5(a), and the FeO contents [21] retrieved from Clementine data [21] are shown in Figure 5(b). It can be seen that the FeO contents of the east Oceanus Procellarum is higher than the west. The low-FeO area is located in the northwest of the test area and high-FeO area lies in the southeast.

The IIM derived FeO contents of the four band selection schemes are shown in Figure 6. The maps of FeO contents retrieved from Clementine (Figure 5(b)) and IIM data (Figure 6) are drawn under the same color scale for comparative purposes. As indicated by the two figures, the distribution patterns of the five FeO maps are similar. However, more detailed information can be identified in Figure 6 because of highly spatial resolution of IIM data. In contrast, the FeO abundance values in each map are inconsistent. FeO content retrieved from 757 nm and 918 nm (Figures 6(b) and (d)) is higher than that from 757 nm and 891 nm (Figures 6(a) and (c)). One possible reason is that band 891 nm and 918 nm represents different Fe absorption characteristic. The absorption center of mafic minerals is located around 940–1000 nm, and 918 nm is closer to it. Figure 6(a) shows the lowest FeO content which is retrieved from IIM 757 nm and 891 nm band without performing cross-calibration. The map with highest FeO contents is Figure 6(b) which is retrieved by IIM 757 nm and 918 nm bands, without performing cross-calibration as well. Both Figures 6(a) and (b)

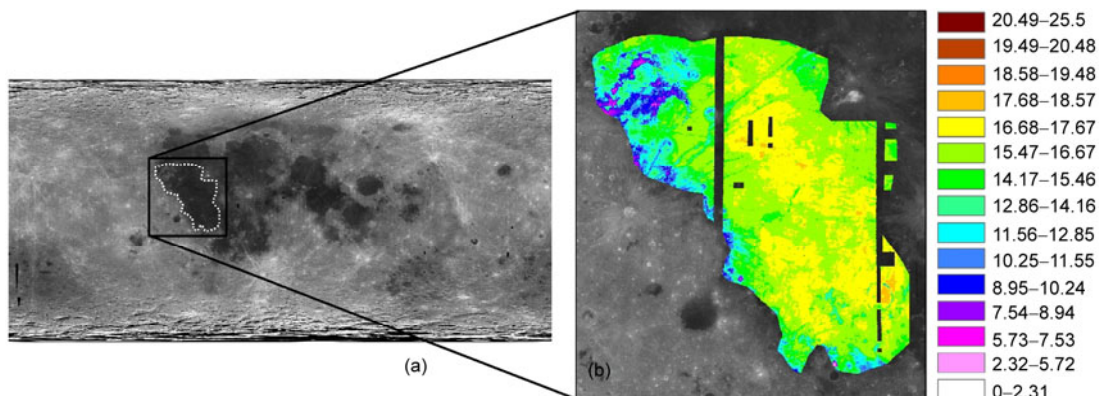


**Figure 5** Sketch map of Oceanus Procellarum area (a) and FeO contents derived from Clementine multispectral data ((b), from Lucey et al. [21]).

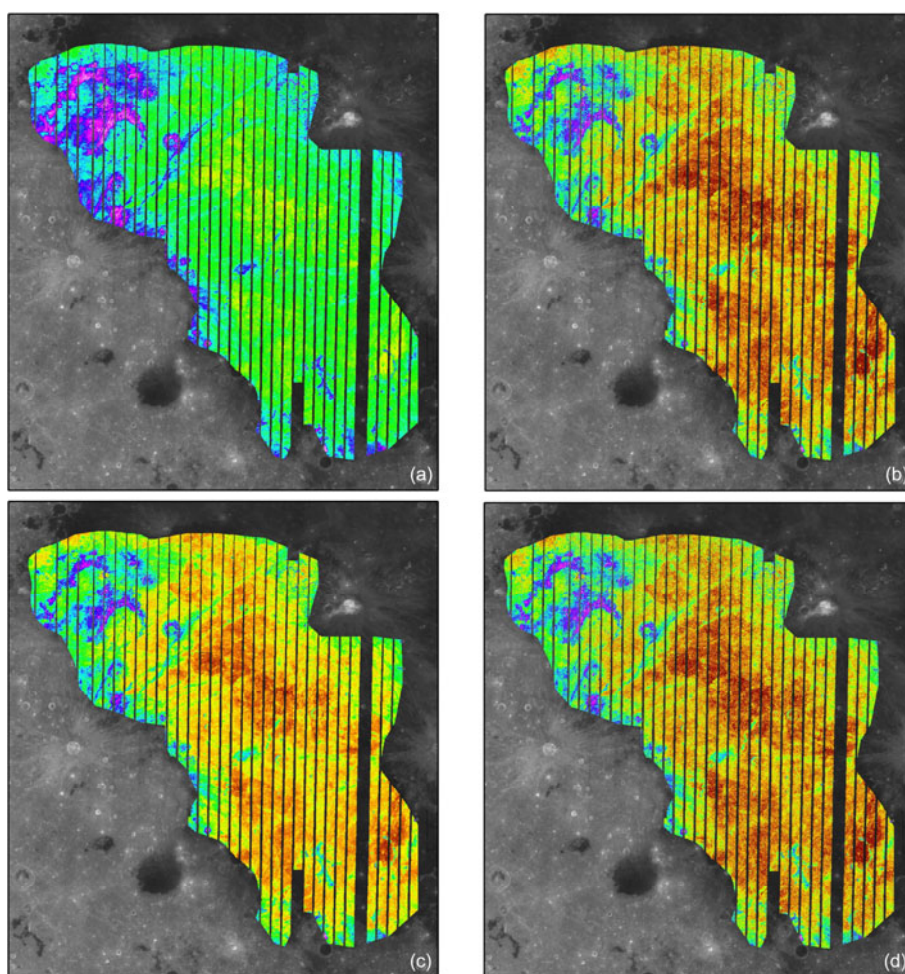


**Figure 6** Maps of FeO contents retrieved from the four schemes: 757 nm and 891 nm without cross-calibration (a), 757 nm and 918 nm without cross-calibration (b), 757 nm and 891 nm with cross-calibration (c), 757 nm and 918 nm with cross-calibration (d).

show a large difference to Clementine derived FeO (Figure 4(b)). The colors of Figure 6(c) are most consistent to Clementine derived FeO contents which represents the real FeO values.

The histograms of the five FeO maps (Clementine and IIM derived FeO) are plotted in Figure 7. The black curve

represents the histogram of Clementine derived FeO (from Figure 5(b)). The red and green curves represent the histograms of FeO retrieved from IIM spectra without applying cross-calibration (Figures 6(a) and (b)) and the blue and yellow curves represent the histograms of FeO retrieved from IIM with applied cross-calibration (Figures 6(c) and

(d). The five histograms all have an approximate normal distribution. Peak value of Clementine derived FeO histogram is at 16.61wt%. The four peak values of IIM derived FeO are located at 14.75wt% (Figure 6(a)), 18.37wt% (Figure 6(b)), 17.92wt% (Figure 6(c)) and 18.22wt% (Figure 6(d)). The blue and yellow curves follow closer to the black curve than the red and green, which suggests that the cross-calibration improved the accuracy of the FeO inversion. The distance between the peak values of IIM derived FeO to Clementine FeO histogram is 1.86, 1.76, 1.31 and 1.61, respectively. The distance between the peak values of the black curve and the blue one is smallest. Considering the same distribution patterns of Clementine FeO data and IIM derived FeO data, we can conclude that the third scheme, using 757 nm and 891 nm band of IIM data with cross-calibration, is the most optimal scheme for FeO inversion. The reason why resultant FeO retrieving from 891 nm is better than 918 nm (with cross-calibration) can be explained by a higher noise in 918 nm band, compared to that in 891 nm band. Figure 8 shows images of IIM 891 nm and

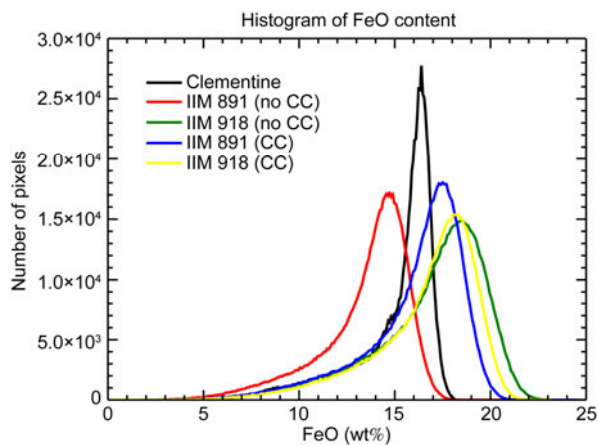


**Figure 7** Histograms of Clementine derived FeO contents and IIM derived FeO contents in Oceanus Procellarum area, CC represents cross calibration.

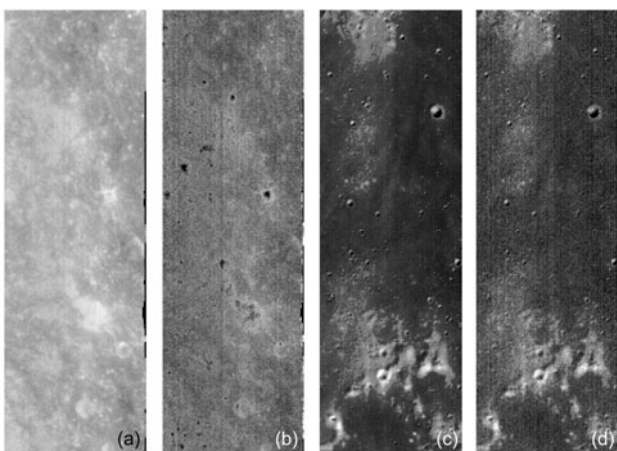


**Figure 8** Images of band 891 nm ((a) and (c)) and 918 nm ((b) and (d)) in highland ((a) and (b)) and mare ((a) and (d)).

918 nm band in two representative types of lunar surface, highland and mare. Because of low SNR, less information is recognized in 918 nm than 891 nm.

## 4 Conclusion

Because of high spatial resolution and spectral resolution, IIM hyperspectral data can be used to detect elements and mineral of the Moon surface at a refined scale. The preprocessing of IIM hyperspectral data is important for research application. IIM spectra suffer from weak response in NIR bands which are vital to iron element inversion and mineral identification. In order to better calibrate the NIR bands, cross-calibration was implemented to IIM hyperspectral data for improving the response. Spectra of twenty-two sites where telescope measured were selected carefully to calculate the cross-calibration factors from 678 nm to 918 nm bands. IIM data at the sites of 22 telescopic spectra were cross-calibrated using these calibration factors. The comparative results between the cross-calibrated IIM spectra and the telescopic spectra show that the weak response in NIR bands has been improved significantly. Concurrently, the correction procedure remains the original spectral feature in IIM short wave bands, which does not need to be corrected. The cross-calibrated results yield consistent results and the cross-calibration procedure has been improved than previous work reported.

In order to show the improvement of utility of IIM data after cross-calibration and seek for the optimal bands for FeO inversion, four band selection schemes were tested to derive FeO contents in Oceanus Procellarum area. By comparing the IIM derived results with Clementine derived FeO in distribution patterns and histograms, the results show that the accuracy of retrieval is improved after cross-calibration, and IIM derived FeO using 757 nm and 891 nm bands is more consistent with the Clementine derived results.

In summary, cross-calibration preprocessing is necessary and positive for IIM data application. Band 891 nm with cross-calibration is recommended for the FeO inversion. The study in this paper promotes the usage of the IIM data and provides a better data source to allow a better understanding of the Moon and the origin and evolution process.

*The authors would like to thank the reviewers for valuable comments and suggestions. Acknowledgement is also given to the Ground Segment for Data, Science and Application (GSDSA) of Chinese Lunar Exploration Program for usage of IIM 2A-level data. This work was supported by the National Basic Research Program of China (Grant No. 2010CB951603), Shanghai Science and Technology Support Program Special for EXPO (Grant No. 10DZ0581600), the Open Research Funding Program of KLGIS (Grant No. KLGIS2011A09), the National Natural Science Foundation of China (Grant No. 41172296) and the Program for New Century Excellent Talents in University (Grant No. NCET-11-0242).*

- Chang'E-1 lunar orbiter: Based on payloads detection data in the first phase. *Chin J Space Sci*, 2008, 5: 361–369
- 2 Xue B. Study on Information Processing and Application of CE-1 Interference Imaging Spectrometer. Dissertation for Doctoral Degree. Xi'an: Institute of Optics and Precision Mechanics, Chinese Academy of Sciences, 2006. 58–59
  - 3 Pieters C M. The Moon as a calibration standard enabled by lunar samples. In: *New Views of the Moon II: Understanding the Moon Through the Integration of Diverse Datasets*, Flagstaff. 1999, Abstract No. 8025
  - 4 Pieters C M, Pratt S. Earth-based near-infrared collection of spectra for the Moon: A new PDS data set. *Lunar Planet Sci XXXI*, 2000, 2059
  - 5 Tsuneko M, Makiko O, Junichi H, et al. Discoveries on the lithology of lunar crater central peaks by SELENE Spectral Profiler. *Geophys Res Lett*, 2008, 35: L23201
  - 6 Wu Y Z, Xu X S, Xie Z D, et al. Absolute Calibration of the Chang'E-1 IIM camera and its preliminary application. *Sci China Ser G-Phys Mech Astron*, 2009, 39: 1378–1392
  - 7 Wu Y Z, Zhang X, Yan B K, et al. Global absorption center map of mafic minerals on the Moon as viewed by CE-1 IIM data. *Sci China-Phys Mech Astron*, 2010, 53: 2160–2171
  - 8 Wu Y Z, Zheng Y C, Zou Y L, et al. A preliminary experience in the use of Chang'E-1 IIM data. *Planet Space Sci*, 2010, 58: 1922–1931
  - 9 Wu Y Z, Besse S, Li J Y, et al. Photometric correction and in-flight calibration of Chang'E-1 Interference Imaging Spectrometer (IIM) data. *Icarus*, 2013, 222: 283–295
  - 10 Wu Y Z, Xue B, Zhao B C, et al. Global estimates of lunar iron and titanium contents from the Chang'E-1 IIM data. *J Geophys Res*, 117: E02001, doi: 10.1029/2011JE003879
  - 11 Pieters C M, Pratt S. Earth-based near-infrared collection of spectra for the Moon: A new PDS data set. In: *Lunar Planet Sci*, XXXI, Abstract 2059
  - 12 Lucey P G, Taylor G J, Malaret E. Abundance and distribution of iron on the Moon. *Science*, 1995, 268: 1150–1153
  - 13 Taylor R S. The unique lunar composition and its bearing on the origin of the Moon. *Geochim Cosmochim Acta*, 1987, 51: 1297–1309
  - 14 Elphic R C, Lawrence D J, Feldman W C, et al. Lunar rare earth element distribution and ramifications for FeO and TiO<sub>2</sub>: Lunar prospector neutron spectrometer observations. *J Geophys Res*, 2012, 105(E8): 20333–20345
  - 15 Ling Z C, Zhang J, Liu J Z, et al. Preliminary results of FeO mapping using Imaging Interferometer data from Chang'E-1. *Chin Sci Bull*, 2011, 56: 376–379
  - 16 Yan B K, Xiong S Q, Wu Y Z, et al. Mapping Lunar global chemical composition from Chang'E-1 IIM data. *Planet Space Sci*, 2012, 67: 119–129
  - 17 Zhao B C, Yang J F, Chang L Y, et al. Optical design and on-orbit performance evaluation of the imaging spectrometer for Chang'E-1 lunar satellite. *Acta Photon Sin*, 2009, 38: 479–483
  - 18 Pieters C M, Stankevich D G, Shkuratov Y G, et al. Statistical analysis of the links among lunar mare soil mineralogy, chemistry, and reflectance spectra. *Icarus*, 2002, 155: 285–298
  - 19 Wu Y Z. Major elements and Mg# of the Moon: Results from Chang'E-1 Interference Imaging Spectrometer (IIM) data. *Geochim Cosmochim Acta*, 2012, 93: 214–234
  - 20 Zhang X Y, Li C L, Lü C. Quantification of the chemical composition of lunar soil in terms of its reflectance spectra by PCA and SVM. *Chin J Geochem*, 2009, 28: 204–211
  - 21 Lucey P G, Blewett D T, Hawke B R. Mapping the FeO and TiO<sub>2</sub> content of the lunar surface with multispectral imagery. *J Geophys Res*, 1998, 103(E2): 3679–3699
  - 22 Lucey P G, Blewett D T, Jolliff B L. Lunar iron and titanium abundance algorithms based on final processing of Clementine ultraviolet-visible images. *J Geophys Res*, 2000, 105(E8): 20297–20305
  - 23 Gillis J J, Jolliff B L. A revised algorithm for calculating TiO<sub>2</sub> from Clementine UVVIS data: A synthesis of rock, soil, and remotely sensed TiO<sub>2</sub> concentrations. *J Geophys Res*, 2003, 108: E2
  - 24 Lucey P G, Blewett D T. Some issues related to lunar FeO and TiO<sub>2</sub>. *Lunar Planet Sci*, 1997, 28: 841–842
  - 25 Zhou X F, Zhao S H, Wu Y Z, et al. Research on extraction of FeO and TiO<sub>2</sub> contents of the Sinus Iridum area based on various optical remote sensing data (in Chinese). *Sci Sin-Phys Mech Astron*, in press